Continuous human activity recognition for arbitrary directions with distributed radars

Guendel, Ronny Gerhard; Unterhorst, Matteo; Gambi, Ennio; Fioranelli, Francesco; Yarovoy, Alexander

DOI
10.1109/RadarConf2147009.2021.9454972

Publication date
2021

Document Version
Final published version

Published in
2021 IEEE Radar Conference

Continuous human activity recognition for arbitrary directions with distributed radars

Ronny Gerhard Guendel*, Matteo Unterhorst†, Ennio Gambi†, Francesco Fioranelli*, Alexander Yarovoy*
*Microwave Sensing, Signals and Systems (MS3), Delft University of Technology, Delft, Netherlands
†Dipartimento di Ingegneria dell'Informazione, Universita' Politecnica delle Marche, Ancona, Italy

2021 IEEE Radar Conference (RadarConf21) | 978-1-7281-7609-3/20/$31.00 ©2021 IEEE | DOI: 10.1109/RadarConf2147009.2021.9454972

***Abstract*—Continuous Activities of Daily Living (ADL) recognition in an arbitrary movement direction using five distributed pulsed Ultra-Wideband (UWB) radars in a coordinated network is proposed. Classification approaches in unconstrained activity trajectories that render a more natural occurrence for Human Activity Recognition (HAR) are investigated. Feature and decision fusion methods are applied to the priorly extracted handcrafted features from the range-Doppler. A following multinomial logistic regression classifier, commonly known as Softmax, provides explicit probabilities associated with each target label. The outputs of these classifiers from different radar nodes were combined with a probability prediction balancing approach over time to improve performances. The final results show average improvements between 6.8% and 17.5% compared to the usage of any single radar in unconstrained directions.**

***Index Terms*—Micro-Doppler Classification, Distributed Radar, Machine Learning, Assisted Living, Human Activity Recognition.**

I. Introduction

Technologies for monitoring Activities of Daily Living (ADL), including radar, can support safe and independent "ageing-in-place" for vulnerable population [1]–[3]. These technologies can provide prompt detection of critical events such falls, but also of abnormalities emerging over time, for example gait impairments during walking [4]. Furthermore, patterns of daily activities can shed light on physical and psychological well-being states for people monitored.

In this field, several trends have gained recently attention in the literature. For example, information fusion across multiple sensors, including cases of contactless radar technology together with wearable devices [5]. Equally important is the recognition of continuous and consecutive ADL apart from single-recorded activities. In this respect, researchers have demonstrated detecting sequences of ADLs by using deep learning techniques, such as the long short-term memory (LSTM) [6]. Also, state separation between translational and in-place activities was introduced for the usage of dynamic classifiers increasing the performance with backward in time classification and "re-visiting of activities" [7]–[9]. Other promising results showed a categorization of different walking gaits in unconstrained directions associated to different subjects [10].

To expand those studies, we propose here a methodology for classifying continuous and sometimes contiguous ADL in arbitrary movement directions by using a coordinated radar network. To the best of our knowledge, Human Activity Recognition (HAR) in unconstrained directions and in a radar network has rarely been considered, since it introduces a variety of challenges, i.e., radar synchronization, interference issues, choice of optimal radar location and data fusion.

We approach this problem with a distributed radar network with nodes located in a circular baseline with 45° separation angle from each other. Five identical pulsed Ultra-Wide Band (UWB) radars are used with a circular measuring space for unconstrained activities of approximately 4.39m, as shown in Fig. 1 with the radar laboratory at TU Delft. To leverage the multi-perspective views enabled by the radar network, suitable information fusion approaches are investigated, specifically feature and decision level fusion operating on seven features extracted from range-Doppler (RD) maps generated by each radar. Multinomial logistic regression classifiers–Softmax classifiers–are used to exploit in the information fusion process with the explicit probabilities associated to all class labels provided by these classifiers. Performance improvements in the overall classification results are reported when using a probability balancing method to concatenate multiple outputs from the Softmax classifiers across multiple radar nodes and multiple slow-time bins. We prove that the proposed classification framework applied on test sequences of unconstrained ADLs improves performances between 6.8% and 17.5%, in comparison to using only individual radars.

The main contribution of this paper includes a classification approach for unconstrained activity recognition. This uses information fusion implemented as Softmax class probability balancing over slow-time bins and across multiple radar nodes.

The rest of the paper is organized as follows. Section II describes the experimental setup, data collection and features extracted. Section III introduces the Softmax classifiers, the fusion models, and the probability prediction balancing methods for improving robustness. In Section IV the results of the different classification approaches are discussed, with final remarks given in Section V.

II. Experimental setup and data representation

The section introduces the ADLs included in the dataset together with the features extracted from the RD maps. The activities were performed in an arbitrary movement trajectory and recorded simultaneously with five radars. The placement of the radars is visualized in Fig. 1 with a height of 1m above ground for a measuring circular space of approximately 4.39m.

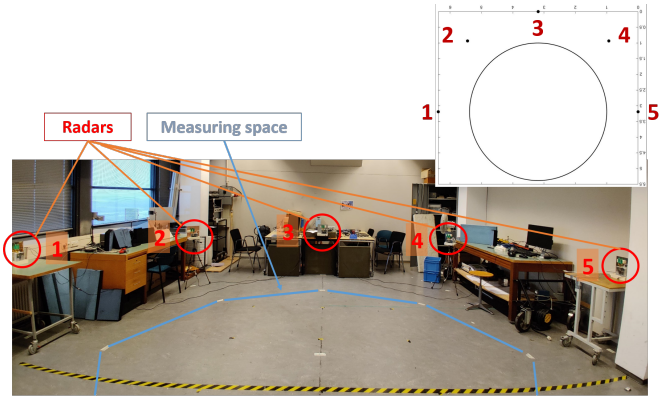

Fig. 1: Radar network layout at TU Delft MS3 lab with a measuring space of about 4.39m.

A. Radar setting and features extracted

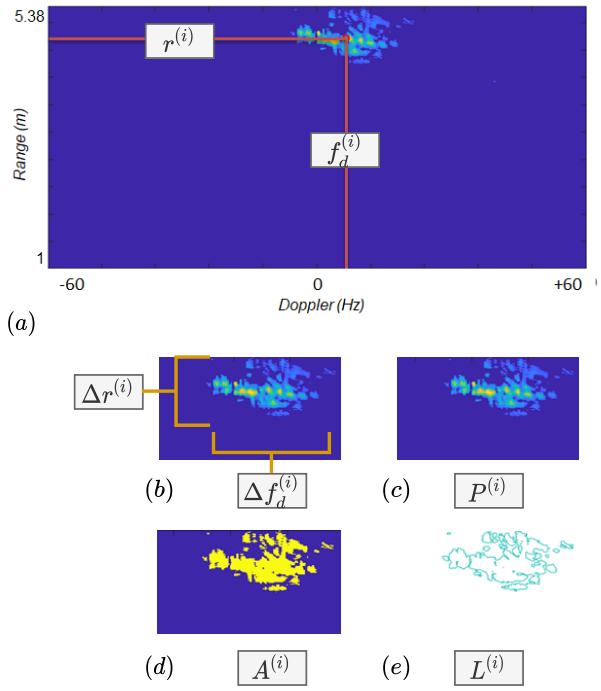

Fig. 2: The 7 features extracted from RD maps: (a) Doppler frequency & range peak power; (b) Doppler width & range width; (c) weighted area; (d) area; (e) perimeter length.

The data set was recorded with Humatics (former PulsON) P410 pulsed radar systems with a f_{PRF} of 122Hz (PRI: 8.2ms). The unambiguous Doppler frequency results in ± 61 Hz (± 2.2 m/s) [11]–[13]. A variety of different FFT window sizes and step-widths between consecutive RD maps were tested. Clutter cancelation is perfromed by subracting the mean RD matrix evaluated from the training set. Finally, superior classification was achieved by the RD step-width of 10 samples (82ms) and a window of 150 samples (1.23s). It was noted, a step-width less than 5 samples did not provide classification advantages. A RD threshold of 80% was used to eliminate the noise, with the result shown in Fig. 2a. The seven extracted features are:

Fig. 2a	Doppler peak-power frequency	:=	$f_d^{(i)}$
Fig. 2a	Range peak-power	:=	$r^{(i)}$
Fig. 2b	Doppler width (x-width)	:=	$\Delta f_d^{(i)}$
Fig. 2b	Range width (y-width)	:=	$\Delta r^{(i)}$
Fig. 2c	Weighted area (Strength)	:=	$P^{(i)}$
Fig. 2d	Area	:=	$A^{(i)}$
Fig. 2e	Perimeter length	:=	$L^{(i)}$

The features of the Doppler peak-power frequency, $f_d^{(i)}$, and the range peak-power, $r^{(i)}$, are determined by the maximum peak power sample after noise-cancellation threshold (Fig. 2a). The Doppler width, $\Delta f_d^{(i)}$, is found by the rising energy after summing the Doppler-bins, and the range width feature, $\Delta r^{(i)}$, by the rising energy after summing the range-bins (Fig. 2b). The area, $A^{(i)}$, is the sum of the logical pixel (0 or 1) of the RD map (Fig. 2d). The weighted area (strength), $P^{(i)}$, is the sum of the RD samples after thresholding (Fig. 2c). Finally, the Perimeter length, $L^{(i)}$, represents the length of the bounding region (Fig. 2e). The introduced features are concatenated as discussed more later in Section III-B, to obtain the feature vector, $x_n^{(i)}$, equal to $\left[f_{d,n}^{(i)}, r_n^{(i)}, \Delta f_{d,n}^{(i)}, \Delta r_n^{(i)}, A_n^{(i)}, P_n^{(i)}, L_n^{(i)}\right]^T$, for each radar node n, at sample time i.

B. Dataset description

The collected dataset consists of 9 classes, namely:

1) Walking
2) Stationary (almost no movement)
3) Sitting down
4) Standing up (from sitting)
5) Bending (while sitting)
6) Bending (while standing)
7) Falling (while walking)
8) Standing up (after falling)
9) Falling (while standing stationary)

We recorded seven *training data* sequences and one *test data* sequence for five subjects, respectively. The training sequence has a total duration of 8 min (4×2 min). It is noted that some sequences contain two activities in pair, i.e., "sitting down" and "standing up from sitting", and similarly "falling" and "standing up after falling". The class "stationary" is contained in all sequences, i.e., at the transition between different activities, while stopping during the walking sequence, or pausing while sitting.

Separately recorded *test sequences* of 2 min for each subject contain all nine activities listed before, but in a different order compared to the training sequences. The order of the activities in the *test sequences* is shown in Fig. 4.

III. Classification Approach

The proposed classification approach uses multinomial logistic regression classifiers – also called *Softmax* – to obtain labels and probabilities for classes of interest, followed by

fusion models and *probability prediction balancing* to effectively combine information from multiple radars. For fusion, feature level and two decision level models are described in this section and depicted in Fig. 3.

A. The Softmax classifier

The Softmax classifier is a probability driven regression model. It can be seen as an extended logistic regression model and provides explicit probabilities for multiclass problems in addition to the labels. Similar to logistic regression, the Softmax probabilities can be expressed by the following activation function,

$$\hat{p}_k = \sigma(s\,(x))_k = \sigma\left(x^T\Theta^{(k)}\right) = \frac{\exp\left(x^T\Theta^{(k)}\right)}{\sum\limits_{j=1}^{K}\exp\left(x^T\Theta^{(j)}\right)} \quad (1)$$

with $\hat{p}_k$ the estimated probability for the class k in the class set K. In Eq. 1 the notation includes the parameter vectors $\Theta^{(k)}$, and the feature vectors, x. The score of each class is $\sigma(s\,(x))_k$ for the instance, $x^T\Theta^{(k)}$.

The classifier works for each classification prediction by determining the highest estimated probability as,

$$\hat{y} = \underset{k}{argmax}\,[\hat{p}_k] \quad (2)$$

for a predicted class $\hat{y}$ [14].

B. Fusion models for distributed radars

Classification with the Softmax classifier can be performed in different ways. In this section three different fusion methods are introduced, with each method providing the predicted class, $\hat{y}^{(i)}$.

For that, we introduce, $\kappa_{m,n}^{(i)}$, denoting the individual feature samples, with the index i for the time sample index; $\{m|1,...,M\}$ for the individual feature from 1 to 7; and $\{n|1,...,N\}$ for the individual radar from 1 to 5.

The first method is commonly known as feature fusion or early fusion by concatenating all feature samples from all radars, so that the feature vector $x^{(i)}$ of length 35 (7 features extracted from 5 radars) is formed as $\left[\kappa_{1,1}^{(i)},...,\kappa_{M,1}^{(i)},...,\kappa_{1,N}^{(i)},...,\kappa_{M,N}^{(i)}\right]^T$. For feature fusion, the Softmax classifier provides the single probabilities $\hat{p}_k^{(i)}$ at each time instance i, for the classes k. The highest probability determines the predicted class, $\hat{y}^{(i)}$, by using Eq. 2.

The alternative fusion method is known as decision fusion or late fusion. For that, the classifiers provide N probabilities, $\hat{p}_{k,n}^{(i)}$, from the 5 radars. The feature vectors are $x_n^{(i)}$, containing the features from each radar separately, specifically $\left[\kappa_{1,1}^{(i)},...,\kappa_{M,1}^{(i)}\right]^T$ for $x_1^{(i)}$ belonging to radar 1, up to $\left[\kappa_{1,N}^{(i)},...,\kappa_{M,N}^{(i)}\right]^T$ for $x_N^{(i)}$, belonging to radar N. The probability vectors for decision fusion can be expressed as,

$$\hat{p}_{k,n}^{(i)} = \begin{bmatrix}\hat{p}_{1,n}^{(i)}\\ \vdots \\ \hat{p}_{K,n}^{(i)}\end{bmatrix}, n = 1,\cdots,N \quad (3)$$

with k as the class and i the time instances, for the radar n in the radarset N.

The vector in Eq. 3 is used for the first decision fusion method by fusing the individual radar probabilities based on their mean as,

$$Mean\left(\hat{p}_k^{(i)}\right) = \frac{1}{N}\sum_{n=1}^{N}\hat{p}_{k,n}^{(i)} \quad (4)$$

with n the index of the radars in the set N. As for feature fusion, Eq. 2 provides the predicted class as,

$$\hat{y}^{(i)} = \underset{k}{argmax}\left[Mean\left(\hat{p}_k^{(i)}\right)\right] \quad (5)$$

For the second decision fusion method, median operation is used to fuse the probabilities of individual radars. The elements of $\hat{p}_k^{(i)}$ were sorted according to their values, as $\hat{q}_k^{(i)} = sort\left(\hat{p}_k^{(i)}\right)$, with $(\cdot)_\upsilon$ in the value set Υ, such as,

$$Med\left(\hat{q}_k^{(i)}\right) = \begin{cases} q_{k,\Upsilon/2}^{(i)} & \text{, if } \Upsilon \text{ is odd} \\ \frac{q_{k,(\Upsilon-1)/2}^{(i)} + q_{k,(\Upsilon+1)/2}^{(i)}}{2} & \text{, if } \Upsilon \text{ is even} \end{cases} \quad (6)$$

The final predicted class is then determined as,

$$\hat{y}^{(i)} = \underset{k}{argmax}\left[Med\left(\hat{q}_k^{(i)}\right)\right] \quad (7)$$

C. Probability prediction balancing

The provided probabilities, $\hat{p}_k^{(i)}$, from the Softmax classifier can fluctuate over time, especially for the test sequences. These fluctuations happen regardless of the used fusion model. They may lead to random jumps between the predicted $\hat{y}^{(i)}$ classes. Hence, time filtering of the probabilities increases the classification robustness. We use the term *probability prediction balancing* for probability time filtering.

The balanced probabilities $\overline{\hat{p}_k^{(i)}}$ for each class k and for the i-th time instance from the feature fusion method is computed as,

$$\begin{aligned}\overline{\hat{p}_k^{(i)}} &= \frac{\hat{p}_k^{(i)} + \hat{p}_k^{(i-1)} + \cdots + \hat{p}_k^{(i-w)}}{w} \\ &= \frac{1}{w}\sum_{\beta=0}^{w} p_k^{(i-\beta)}\end{aligned} \quad (8)$$

with β the discrete counter index, and w the balancing window size over consecutive Softmax predictions.

Similarly to Eq. 8, probability prediction balancing was also applied to both decision fusion methods, such as the mean $Mean\left(\hat{p}_k^{(i)}\right)$, as $\overline{Mean\left(\hat{p}_k^{(i)}\right)}$, and the median $Med\left(\hat{q}_k^{(i)}\right)$, as $\overline{Med\left(\hat{q}_k^{(i)}\right)}$, respectively. The predicted classes after probability prediction balancing $\overline{\hat{y}^{(i)}}$ are computed by replacing the variables $(\cdot)_k^{(i)}$ by $\overline{(\cdot)_k^{(i)}}$ in Eq. 2, 5, and 7, respectively, for the different fusion models.

The flowchart in Fig. 3 provides a graphic summary of the methods discussed in this section.

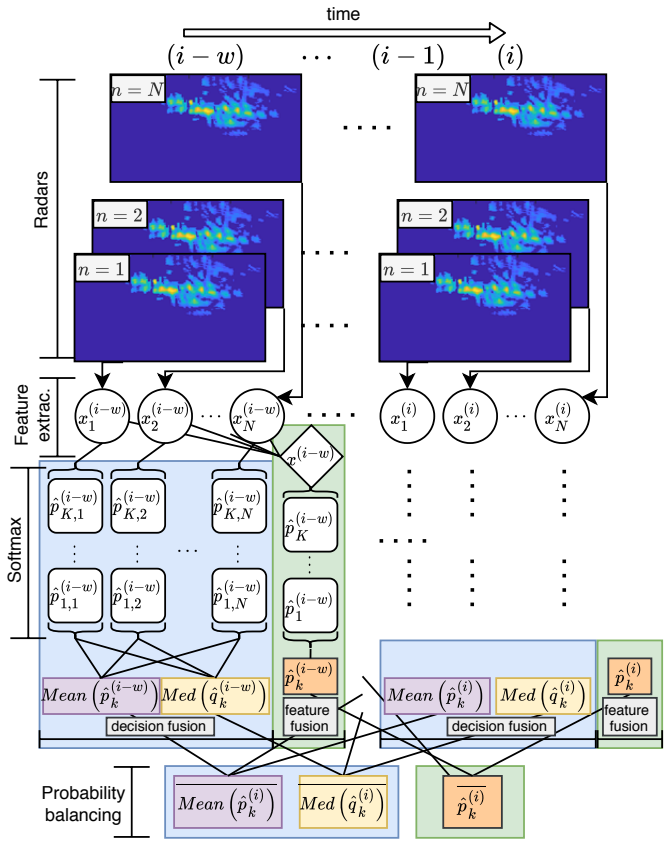

Fig. 3: Flowchart summarizing: feature extraction from range-Doppler, Softmax classifiers, fusion models, and probability prediction balancing across multiple radar nodes.

TABLE I: Softmax classifier validation probabilities for 4 randomly selected activity samples.

Pr	$\hat{p}_1$	$\hat{p}_2$	$\hat{p}_3$	$\hat{p}_4$
GT	**1**	**4**	**7**	**9**
1	**97.51**	0.89	0.26	0.04
2	0.02	1.24	0	0.11
3	0.25	14.12	0.01	6.09
4	0.19	**27.31**	0	4.27
5	1.77	18.21	0.19	0.21
6	0.06	15.29	0	0.4
7	0.12	0.68	**96.58**	20.28
8	0.05	12.91	1.99	18.47
9	0.01	9.35	0.97	**50.14**

IV. Results for different test methodologies

As an example of the probability outputs provided by the Softmax classifier, we show in Table I four random samples from validating the Softmax classifier. We picked four samples from the classes (1) walking, (4) standing up from sitting, (7) falling from walking, and (9) falling from standing. It can be seen that walking has a high prediction accuracy (97.51%) with almost no confusion versus another class. Differently, in the second example of standing up from sitting (27.31%),

TABLE II: Softmax classifier test probabilities of one randomly selected sample from each true class.

Pr	$\hat{p}_1$	$\hat{p}_2$	$\hat{p}_3$	$\hat{p}_4$	$\hat{p}_5$	$\hat{p}_6$	$\hat{p}_7$	$\hat{p}_8$	$\hat{p}_9$
GT	**1**	**2**	**3**	**4**	**5**	**6**	**7**	**8**	**9**
1	**54.2**	0.0	0.6	0.2	0.2	2.1	0.3	29.9	1.4
2	1.1	**75.2**	1.8	22.2	13.4	2.2	0.0	0.6	0.1
3	5.7	6.0	**27.9**	9.9	17.1	16.2	0.0	5.0	4.3
4	4.4	6.5	19.7	**9.8**	13.8	23.4	0.0	7.8	6.4
5	0.7	9.3	7.3	37.1	**28.3**	11.0	0.0	10.6	2.1
6	4.7	1.3	24.3	12.3	20.2	**27.9**	0.0	2.9	10.9
7	1.2	0.1	0.4	0.5	0.4	0.9	**93.0**	2.8	3.7
8	10.9	1.5	10.8	5.7	4.4	8.1	3.4	**21.7**	20.6
9	17.1	0.2	7.2	2.3	2.1	8.2	3.2	18.7	**50.6**

potential confusion is shown towards other classes, such as sitting down (14.12%), bending from sitting (18.21%), or bending from standing (15.29%).

Such confusion in this subset of the four classes occurs because, i.e., sitting down has a close correlation with standing up if the person is 180° turned around. This happens to both the Doppler speed and range extent for arbitrary activity directions. However, depending on the application, confusion among these classes may not be critical as they are not life-threatening actions. In contrast, the latter two samples show life-threatening actions, such as falling from walking and falling from standing, respectively. Notably, almost no confusion is reported in this case. In summary, when assessing performances, confusion in some classes is less critical than in others and can sometimes be tolerated.

Similar observations were seen by comparing the probabilities from a test sequence, where we picked one sample from each class randomly, as in Table II. The previous observation holds, i.e. some classes such as walking, stationary, or falling have higher prediction accuracy than other in-place classes.

In the rest of this section, we demonstrate our methods on two different test modalities:

- *Test subjects included in the training set*
- *Test subjects excluded from the training set*

Typically, the latter case of "Leave One Person Out" performs worse than the former, but is a more robust methodology for testing classification approaches.

A. Test subjects included in the training set

TABLE III: The fusion methodology accuracies with the related prediction balancing window, $\{\cdot\}$, to Fig. 5 and 6.

Description	include person		leave person out	
Feature fusion	55.72%	{14}	52.11%	{15}
Decision fusion (mean)	54.96%	{9}	51.79%	{10}
Decision fusion (median)	53.66%	{10}	50.88%	{12}
Highest single radar	48.17%	{14}	45.29%	{13}

Typical results for the first test modality are shown in Fig. 4a. For a given test sequence we show the results for the

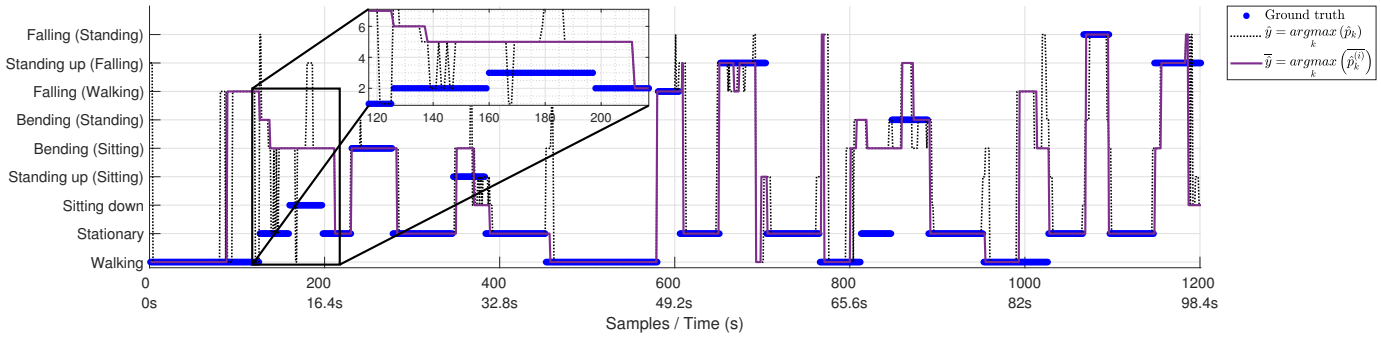

(a) Predicted classes before and after *probability prediction balancing* for an arbitrary sequence with all classes containing.

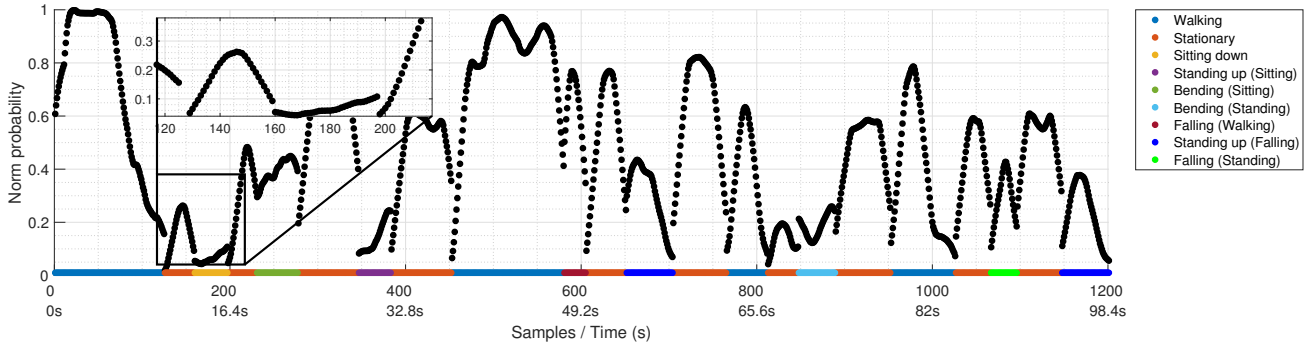

(b) Softmax output probabilities (black) vs ground truth (bottom colored line) as a function of time.

Fig. 4: Unconstrained activity probabilities from Softmax classifier when including the test subject in the training set.

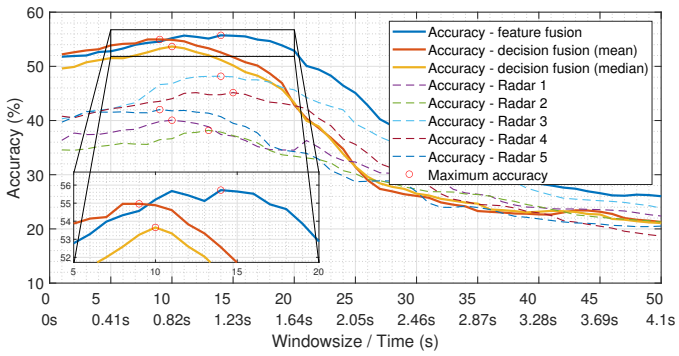

Fig. 5: The fusion methodologies according to the prediction balancing window, with the test subjects included in the training set.

output of the feature fusion model, $\hat{y}$, as the black dotted line. The output after decision fusion with probability prediction balancing of 14 consecutive predictions, $\overline{\hat{y}}$, is also plotted for comparison as the solid purple line. The ground truth is indicated by the blue line. Fig. 4b shows the predicted probability over time for the true classes (indicated by the colour bar at the bottom).

In Fig. 5, the impact of the different fusion models is shown. For all methods, a probability prediction balancing over a certain window improves the classification performance, while feature fusion shows superior results. In contrast, single radar classification is not capable of providing the achieved performance of any fusion model (highest: Feature fusion with 55.72%). Here, radar 3 provides the best average accuracy with 48.17% with a window size of 14 consecutive predictions. The average test accuracies are summarized in Table III, picking the highest value as a function of the window size for probability balancing (Fig. 5).

B. *Test subjects excluded from the training set*

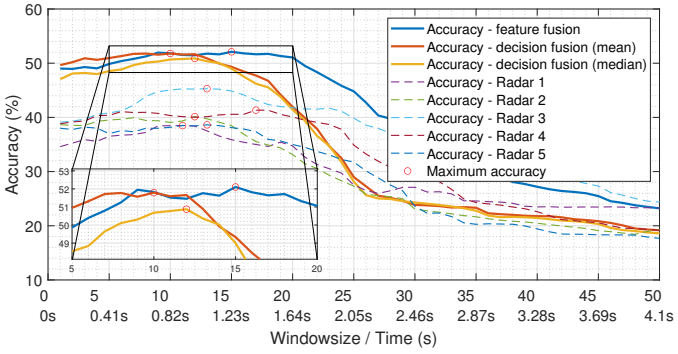

Fig. 6: The fusion methodologies according to the prediction balancing window, with the test subjects excluded from the training set.

The second test modality is based on leaving each test subject out of the training process and assessing the average result across all subjects. A slight decrease in performance is expected, as each individual moves differently even when

performing the same action (human ethogram [15]), hence their feature samples for the same classes will vary as well. Our results show that the average test accuracy drops by approximately 3% in comparison to the first test modality, as shown in Table III. The best result of 52.11% was achieved with balancing 15 (window size) consecutive predictions with feature fusion. Furthermore, decision fusion in both applications can almost compete with feature fusion, with 51.79% and 50.88%, respectively. The best average accuracy, 45.29%, for a single radar was achieved with 13 consecutive Softmax predictions, whereas other radars show performances below 40% average accuracy.

In Fig. 6 the effect of varying the number of time bins for balancing prediction probabilities is demonstrate. Specifically, the curves flatten within the window size between 8 and 15 samples for feature fusion. In fact, feature fusion can be seen as the most robust method in terms of the prediction as a function of the window size.

C. Discussion

When classifying realistic, continuous sequences of activities, a discussion is needed to assess the results beyond accuracy metrics typically used for the classification of individual, separated activities. In Fig. 4b the prediction probability is shown over time to help assess the results.

In some cases, as around sample 215, the "stationary" class was identified correctly but with a delay of some samples; in other cases, not shown here for conciseness, there was an anticipation of few samples, perhaps due to errors in ground-truth labelling. While our accuracy calculation is performed on each time sample (or over a window of a certain number of samples as in Table III), it may make more sense assessing correct/wrong transitions between activities rather than assessing individual time samples. This also accounts for the fact that some activities and classes are inherently continuous, i.e. spread over many time samples (e.g. walking, or stationary), whereas others are one-off actions (e.g. sitting, bending). In first instance, detecting these activities in the sequence can be a sufficient outcome, rather than focusing on their duration in terms of time samples that are much shorter (tens of ms) than normal human kinematics.

Different is the case where actual misclassification happens, as around samples 160 and 195 when the prediction of "sitting down" and "bending from sitting" were confused. While this is a mistake reducing the overall accuracy for the way we set up this classification problem, one may argue that it is not a critical mistake: the person was still sitting, no dangerous events like a fall were missed nor false alarms raised. In summary, the definition of accuracy used in this section and uncritically taken from conventional individual, separated activities analysis, may need a refresh in future work extending this analysis of continuous sequences of activities. Still, average test prediction accuracy above 50% for 9 classes are acceptable preliminary results compared to e.g. $\approx 70\%$ for 5 classes of different walking gaits in [10].

V. Conclusion

In this paper, we propose a distributed sensing approach classify Activities of Daily Living in arbitrary movement directions. With a radar network consisting of 5 UWB nodes, average classification improvements between 6.8% and 17.5% compared to single radar classification are demonstrated. The Softmax (multinomial logistic regression) classifier was used in conjunction with feature and decision fusion approaches to combine information across multiple radars, as well as over multiple time bins for improved robustness. These methods were evaluated on experimental data including nine activities performed along unconstrained trajectories. Feature fusion shows the best and most robust results, closely followed by decision fusion, with both significantly outperforming the use of single radars.

References

[1] S. A. Shah and F. Fioranelli, "RF sensing technologies for assisted daily living in healthcare: A comprehensive review," *IEEE Aerospace and Electronic Systems Magazine*, vol. 34, no. 11, pp. 26–44, Nov 2019.

[2] M. G. Amin, A. Ravisankar, and R. G. Guendel, "RF sensing for continuous monitoring of human activities for home consumer applications," in *Big Data: Learning, Analytics, and Applications*, May 2019.

[3] J. Le Kernec, F. Fioranelli, C. Ding, H. Zhao, L. Sun, H. Hong, J. Lorandel, and O. Romain, "Radar signal processing for sensing in assisted living: The challenges associated with real-time implementation of emerging algorithms," *IEEE Signal Processing Magazine*, vol. 36, no. 4, pp. 29–41, July 2019.

[4] A. Seifert, M. G. Amin, and A. M. Zoubir, "Toward unobtrusive in-home gait analysis based on radar micro-Doppler signatures," *IEEE Transactions on Biomedical Engineering*, vol. 66, no. 9, pp. 2629–2640, 2019.

[5] H. Li, X. Liang, A. Shrestha, Y. Liu, H. Heidari, J. Le Kernec, and F. Fioranelli, "Hierarchical sensor fusion for micro-gestures recognition with pressure sensor array and radar," *IEEE Journal of Electromagnetics, RF and Microwaves in Medicine and Biology*, pp. 1–1, 2019.

[6] M. Wang, Y. D. Zhang, and G. Cui, "Human motion recognition exploiting radar with stacked recurrent neural network," *Digital Signal Processing*, vol. 87, pp. 125 – 131, 2019.

[7] M. G. Amin and R. G. Guendel, "Radar classifications of consecutive and contiguous human gross-motor activities," *IET Radar, Sonar Navigation*, vol. 14, no. 9, pp. 1417–1429, 2020.

[8] R. G. Guendel, F. Fioranelli, and A. Yarovoy, "Derivative target line (DTL) for continuous human activity detection and recognition," in *2020 IEEE Radar Conference*, Sept 2020, p. 6.

[9] M. G. Amin and R. G. Guendel, "Radar human motion recognition using motion states and two-way classifications," in *2020 IEEE International Radar Conference (RADAR)*, 2020, pp. 1046–1051.

[10] B. Vandersmissen, N. Knudde, A. Jalalvand, I. Couckuyt, A. Bourdoux, W. De Neve, and T. Dhaene, "Indoor person identification using a low-power FMCW radar," *IEEE Transactions on Geoscience and Remote Sensing*, vol. 56, no. 7, pp. 3941–3952, 2018.

[11] Y. He, P. Aubry, F. Le Chevalier, and A. Yarovoy, "Decentralised tracking for human target in multistatic ultra-wideband radar," *IET Radar, Sonar Navigation*, vol. 8, no. 9, pp. 1215–1223, 2014.

[12] A. Petroff, "A practical, high performance ultra-wideband radar platform," in *2012 IEEE Radar Conference*, 2012, pp. 0880–0884.

[13] Y. He, P. Molchanov, T. Sakamoto, P. Aubry, F. Le Chevalier, and A. Yarovoy, "Range-Doppler surface: a tool to analyse human target in ultra-wideband radar," *IET Radar, Sonar Navigation*, vol. 9, no. 9, pp. 1240–1250, 2015.

[14] A. Geron, *Hands-on machine learning with Scikit-Learn and TensorFlow : concepts, tools, and techniques to build intelligent systems*. O'Reilly Media, 2017.

[15] M. G. Amin, "Micro-Doppler classification of activities of daily living incorporating human ethogram," in *Radar Sensor Technology XXIV*, K. I. Ranney and A. M. Raynal, Eds., vol. 11408, International Society for Optics and Photonics. SPIE, 2020, pp. 42 – 49.